



**ARTICLE**

# Study on Mechanical Properties and Action Mechanism of Leather Industrial Sludge Aggregate Baking-Free Bricks

Lei Guo<sup>1,2,3</sup>, Zekun Wang<sup>1</sup>, Lixia Guo<sup>1,2,3,\*</sup> and Pingping Chen<sup>1</sup>

<sup>1</sup>School of Water Conservancy, North China University of Water Resources and Electric Power, Zhengzhou, 450046, China

<sup>2</sup>Henan Water Valley Research Institute, Zhengzhou, 450046, China

<sup>3</sup>Henan Key Laboratory of Water Environment Simulation and Treatment, Zhengzhou, 450002, China

\*Corresponding Author: Lixia Guo. Email: guolx@126.com

Received: 20 April 2022 Accepted: 25 May 2022

## ABSTRACT

Taking an industrial sludge and its preparation of sludge wrap shell aggregates (WSAs) instead of sand to prepare baking-free brick as the research object, the development law of mechanical properties and the influence mechanism of macro and micro characteristic parameters of the bricks under different sludge and WSAs replacement rates were studied through the macroscopic mechanical properties test, with the help of nuclear magnetic resonance (NMR), transmission electron microscopy-energy spectrum and other testing technology and pores and cracks analysis system (PCAS) software. The results showed that the compressive strength of each sample decreased with the increase of sludge content. When the sludge content was less than 30%, it was mainly affected by the water-binder ratio. When the sludge content was more than 30%, it was mainly affected by the sludge content. At the age of 7 days, with the increase in replacement rate of WSAs, the compressive strength of the S10 and S30 groups was higher than that of the control group. The compressive strength of the S50 experimental group was 30.38 MPa, and the loss of compressive strength was slight compared with the control group. The water absorption rate of the 28 days S100 experimental group increased by 10.71% compared with the control group. When the content of WSAs was less than 50%, the holes above 0.1  $\mu\text{m}$  in the brick can be reduced and transformed into smaller holes, with a decreasing trend of the plane porosity of the brick. The microscopic results of the baking-free brick showed that the three-phase system of WSAs-interface transition area-mortar was poorly bonded and delaminated compared with the gravel aggregate-interface transition area-mortar system, and damage was more likely to occur in the WSAs and interface transition area. The above results show that it is feasible to use sludge and WSAs instead of sand for the preparation of baking-free bricks. This technology not only solves the problem of sludge disposal, but also protects the over-exploitation of mineral resources, and the technology has a broad application prospect and market value.

## KEYWORDS

Sludge; wrap shell aggregates; baking-free brick; interface

## Abbreviation

Nuclear magnetic resonance	(NMR)
Pores and cracks analysis system	(PCAS)
Company Limited	(Co., Ltd.)



This work is licensed under a Creative Commons Attribution 4.0 International License, which permits unrestricted use, distribution, and reproduction in any medium, provided the original work is properly cited.

Carr-Purcell-Meiboom-Gill	(CPMG)
Environmental scanning electron microscope	(ESEM)
Wrap shell aggregates	(WSAs)

## 1 Introduction

With the development of China's economic construction, sand and stone aggregate used for building materials production is up to 10 billion tons every year, and the massive exploitation of natural aggregate is bound to cause serious resource shortage and ecological destruction [1]. The outline of China's Thirteenth Five-Year Plan proposes that renewable building materials should be widely used and the proportion of green buildings should be significantly increased [2].

Sludge is a kind of heterogeneous solid precipitation composed of organic debris, bacteria, inorganic particles, and colloid generated in the sewage treatment process, with high water content, large volume, perishability, smelly, and a lot of heavy metals and other substances harmful to the environment [3]. At present, more than 80% of sludge produced in China has not been effectively treated. Untreated or improperly treated sludge can cause serious environmental pollution such as soil pollution and water pollution. In order to effectively solve the problem of industrial sludge, in line with the principle of green development and sustainable development, it is particularly urgent and important to carry out research on the effective utilization of industrial sludge.

Some scholars have tried to apply sludge to the construction industry for a long time. Kaosol [4] studied the mechanical properties and economic effects of preparing hollow concrete blocks by replacing fine aggregate with sludge. The results showed that concrete blocks with 10% and 20% replacement rates met various standards and had good economic benefits. Liu et al. [5] studied the effects of drinking water sludge instead of sand and stone on compressive strength, porosity, wear-resistance, and heavy metal leaching properties of concrete paving bricks. Francisco et al. [6] analyzed the feasibility of using sewage sludge ash in concrete as raw material for making concrete blocks, experimented with sewage sludge ash instead of sand, and carried out physical and mechanical tests. Hameed et al. [7] used broken rock dust and marble sludge powder as fine aggregate for self-compacting concrete. The results showed that the compressive strength increased with the replacement rate of marble sludge powder and the chloride ion permeability decreased. The studies showed that sludge could be utilized to prepare building materials. Ni et al. selected silt to prepare sintered bricks, obtained the optimal process conditions through variable tests, and investigated the heavy metal leaching of the sintered bricks prepared under the conditions to determine their environmental safety [8]. Although the sintering method can improve the partial performance of brick, it produces greenhouse gases such as carbon dioxide, which is not in line with the development concept of green environmental protection [9,10]. Based on environmental protection and sustainable resources, the technology of using solid waste as a raw material to prepare building materials by the non-burning method was prospective. Guo et al. [11] prepared baking-free bricks in slag and sludge as raw material with excellent performance. Baking-free bricks met the performance requirements of solid concrete bricks (MU40). Although the no-burning method can effectively reduce the consumption of resources and reduce the pollution of the environment, there are still some defects in previous studies. Miqueleiz et al. [12] utilized  $Al_2O_3$  as the raw material to prepare baking-free bricks, the maximum water absorption rate of the brick reached 24%, and the compressive strength was lower than 28 MPa. It can be seen from recent reports that brick prepared by the non-burning method could not ensure excellent properties.

Sludge could prepare into aggregate by the shell-wrapped technology, and the baking-free bricks were then prepared for the aggregates from sludge. In this paper, the sludge and WSAs prepared by the shell-wrapped process are used in the field of baking-free brick materials. According to the particle size of sludge fine particles and WSAs, it can be divided into two particle sizes < 5 mm and 5–10 mm. Sand and

gravel aggregate are replaced with different aggregate replacement rates respectively. The macroscopic properties and microscopic phase tests were carried out to study the mechanical properties of the bricks under different aggregate replacement rates and the influence mechanism of macro-micro characteristic parameters, which provides a new way to utilize sludge in building materials.

## 2 Experiment

### 2.1 Raw Materials

The main mechanical properties of P•O42.5 ordinary Portland cement used in the test are shown in Table 1. The slag was purchased from Henan Yulian Power Plant, with a grayish-white appearance. The main oxide components of raw materials are shown in Table 2, and the microscopic morphology is shown in Fig. 1. The alkaline stimulator is granular CaO, purchased from Tianjin Zhiyuan Chemical Reagent Co., Ltd. (China). The water glass  $\text{Na}_2\text{SiO}_3$  was purchased from Bengbu Jingcheng Chemical Co., Ltd. (China) and was diluted twice when used, which was a milky white transparent liquid.

**Table 1:** Physical and mechanical properties of cement

Specific surface area/ ( $\text{m}^2 \cdot \text{kg}^{-1}$ )	Density/ ( $\text{kg} \cdot \text{m}^{-3}$ )	Setting time/ min		Compressive strength/MPa		Flexural strength/MPa	
		Initial	Final	Three days	Twenty-eight days	Three days	Twenty-eight days
348.7	303.5	176	244	35.9	49.6	5.9	8.6

**Table 2:** Chemical constituents of raw material

Chemical constituents/%	CaO	$\text{Fe}_2\text{O}_3$	$\text{SO}_3$	$\text{Al}_2\text{O}_3$	MgO	$\text{SiO}_2$	$\text{K}_2\text{O}$	$\text{Na}_2\text{O}$	LOI	$\text{Gr}_2\text{O}_3$
Cement	51.27	3.65	2.46	9.25	4.98	24.13	0.79	1.95	3.55	-
Slag	0.57	1.94	-	24	1.22	47.6	7.43	-	2.43	-
Sludge	33.6	10.74	15.83	11.76	2.34	10.16	-	1.68	-	6.17

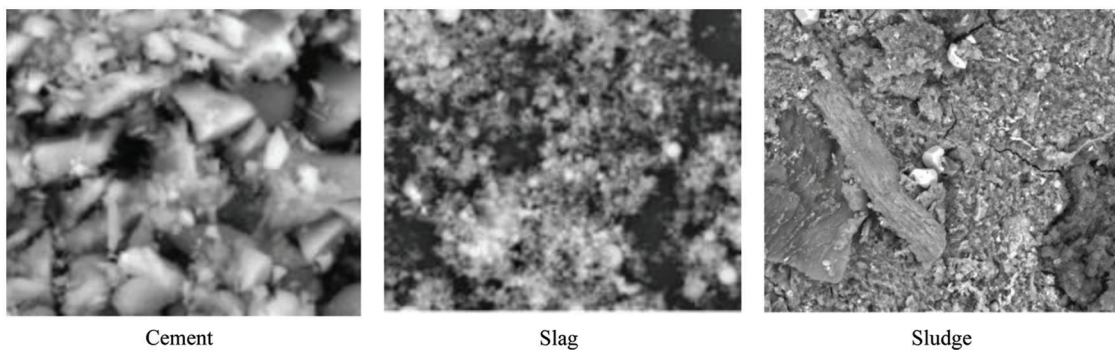


**Figure 1:** Microstructure of cementitious materials

Coarse aggregate gravel was selected with a particle size of 5~10 mm and a bulk density of  $1541.3 \text{ kg/m}^3$ . Medium coarse sand was purchased from Xinmiao Sand and Stone Co., Ltd. (China), with a bulk density of  $1625.0 \text{ kg/m}^3$ , fineness modulus of 3.0 and mud content of 1.5%. The test water was tap water with a pH value of 8.2.

Sludge was taken from a leather factory in Zhumadian City, Henan Province, with high moisture content (up to 99% or more), high organic content, perishable and odorous, containing trace amounts of heavy metal chromium, which was processed as the raw material for the test through the processes of mechanized dewatering, chemical curing, crushing and debris removal. The physical properties of the sludge are shown in Table 3. In this paper, sludge with a particle size of 0.6–4.75 mm is used as fine aggregate instead of sand, and the sludge with a particle size of less than 0.6 mm is prepared into WSAs of 5–10 mm by shell-wrapped process, which is used to replace gravel as coarse aggregate. The aggregate properties prepared by the optimized shell-wrapped process are shown in Table 4.

**Table 3:** Physical properties of sludge

Particle shape	Bulk density/(kg/m <sup>3</sup> )	Fineness modulus	Water absorption/%				Cohesiveness
			10 min	20 min	1 h	24 h	
Polygon	688	3.63	22.08	35.21	37.76	38.27	No

**Table 4:** Physical properties of sludge WSAs

Particle form factor	Bulk density/(kg/m <sup>3</sup> )	Water absorption/%		Cylinder pressure strength/MPa
		1 h	24 h	
1.34	730	12.87	17.04	3.16

Sludge baking-free brick with self-made mold is shown in Fig. 2, with molding specifications of 240 mm × 115 mm × 53 mm, as shown in Fig. 3. By replacing fine aggregate with sludge, the replacement rates were 10%, 30%, and 50%. Sludge WSAs replaced coarse aggregate with replacement rates of 30%, 50%, 70%, 90%, and 100%. The baking-free brick test was designed, and the test mix ratio was shown in Tables 5 and 6. The molding process refers to the existing test [13–15] and adopts vibration and molding mode to imitate the outdoor molding process. The pressure source is the self-made counterweight, and the counterweight is 20 kg. After demolding, the formed specimens were moved to the standard curing room (23 ± 2°C, 95%), and the performance test was conducted after curing for 7, 14, and 28 days.



**Figure 2:** Home mould



**Figure 3:** Baking-free brick specimen

**Table 5:** Test mix ratio of sludge fine aggregate

Test team	Coarse aggregate/ (kg/m <sup>3</sup> )	Sand/ (kg/m <sup>3</sup> )	Sludge/(kg/m <sup>3</sup> ) (replacement rate/%)	Cement/ (kg/m <sup>3</sup> )	Water	
					Water-binder ratio	Quality/ (kg/m <sup>3</sup> )
DZ	900	950	0	320.0	0.42	134.4
S <sub>10</sub> W <sub>0.42</sub>	900	855.0	95.0 (10)	320.0	0.42	134.4
S <sub>30</sub> W <sub>0.42</sub>	900	665.0	285.0 (30)	320.0	0.42	134.4
S <sub>50</sub> W <sub>0.42</sub>	900	475.0	475.0 (50)	320.0	0.42	134.4
S <sub>10</sub> W <sub>0.48</sub>	900	855.0	95.0 (10)	320.0	0.48	153.6
S <sub>30</sub> W <sub>0.48</sub>	900	665.0	285.0 (30)	320.0	0.48	153.6
S <sub>50</sub> W <sub>0.48</sub>	900	475.0	475.0 (50)	320.0	0.48	153.6
S <sub>10</sub> W <sub>0.54</sub>	900	855.0	95.0 (10)	320.0	0.54	172.8
S <sub>30</sub> W <sub>0.54</sub>	900	665.0	285.0 (30)	320.0	0.54	172.8
S <sub>50</sub> W <sub>0.54</sub>	900	475.0	475.0 (50)	320.0	0.54	172.8

**Table 6:** Test mix ratio of sludge WSAs

Test team	Sand/ (kg/m <sup>3</sup> )	Coarse aggregate/ (kg/m <sup>3</sup> )	WSAs/(kg/m <sup>3</sup> ) (replacement rate%)	Cement/ (kg/m <sup>3</sup> )	Water		Additional water	
					Water-binder ratio	Quality/ (kg/m <sup>3</sup> )	Proportion /%	Quality/ (kg/m <sup>3</sup> )
S0	950.0	900.0	0	320.0	0.42	134.4	0	0.0
S10	950.0	810.0	90.0 (10)	320.0	0.42	134.4	10.0	9.0
S30	950.0	630.0	270.0 (30)	320.0	0.42	134.4	10.0	27.0
S50	950.0	450.0	450.0 (50)	320.0	0.42	134.4	10.0	45.0
S70	950.0	270.0	630.0 (70)	320.0	0.42	134.4	10.0	63.0
S90	950.0	90.0	810.0 (90)	320.0	0.42	134.4	10.0	81.0
S100	950.0	0.0	900.0 (100)	320.0	0.42	134.4	10.0	90.0

## 2.2 Test Ratio

The additional water is the amount of pre-water absorption before mixing the WSAs, that is, the WSAs are pre-soaked before the test, the additional water is 10% of the mass of the WSAs, and the aggregate is kept dry during mixing.

## 2.3 Test Method

### 2.3.1 Macroscopic Performance Test

The compressive strength and water absorption of baking-free brick were determined in accordance with “Solid Concrete Bricks” GB/T 21144-2007 and “Test Methods for Concrete Blocks and Bricks” GB/T 4111-2013 [16,17], and the calculation formulas were as follows:

Compressive strength:

$$R_P = \frac{P}{LB} \quad (1)$$

where  $P$  is the maximum failure load,  $L$  is the length of the compression surface, and  $B$  is the width of the compression surface.

Water absorption:

$$\omega = \frac{m_1 - m}{m} \quad (2)$$

where  $m_1$  is the quality of 24 h water absorption of baking-free brick, and  $m$  is the drying quality of baking-free brick.

### 2.3.2 Pore Structure Analysis

In this paper, image processing technology and the NMR pore-measuring method are used to study the pore structure of baking-free brick. The pore size range of NMR is 0.1–200  $\mu\text{m}$ , and the image processing technology can extract the pore size larger than 200  $\mu\text{m}$ . The image processing technology was to slice the baking-free brick test block with a rock cutting machine. After slicing, an industrial camera was used to extract the sliced image. The PCAS software was used to extract the plane porosity and fractal dimension of pores with a diameter of more than 200  $\mu\text{m}$ . The fractal dimension represents the regularity of the pores. The larger the fractal dimension, the more irregular the pore structure [18,19]. The NMR test hole was vacuum saturated by a vacuum pressure saturation device. After the vacuum saturation, the specimen was put into the coil of the NMR instrument, and the NMR relaxation was measured by the EDUMR20-015V-I nuclear magnetic resonance analysis system. After the CPMG sequence attenuation signal data was collected, the T2 spectrum was obtained by data inversion. Subsequently, it was transformed into a pore size distribution map [20,21].

### 2.3.3 Phase Structure Analysis

Take the sample of baking-free brick, retain the original shape, and take a small number of residual pieces with tweezers, with the section facing upward, and fix them on the conductive adhesive of the sample base. After spraying gold coating, the sample is ready for analysis and detection. The instrument is QUANTA 650 environmental Scanning electron microscope (ESEM) from FEI Company (China) and Apollo-X energy spectrometer from EDAX Company (USA). The working voltage is 25 kV, the working distance is 10 mm, and the scanning time is 30 s.

### 3 Results Analysis

#### 3.1 Influence of Sludge Content on Properties of Baking-Free Brick

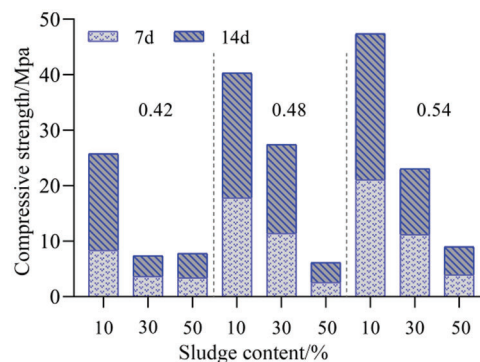
##### 3.1.1 Compressive Strength

Fig. 4 shows the sample pictures of baking-free bricks with different sludge contents. It can be found that the molding quality and appearance of baking-free brick are significantly different with different sludge content. The appearance color of the baking-free brick sample gradually deepens with more sludge content and more defects in specimen appearance.



**Figure 4:** Baking-free brick sample

Fig. 5 shows the influence of different sludge content and water-binder ratio on the compressive strength of baking-free brick at 7 and 14 days. It can be seen from the figure that the compressive strength at the age of 14 days increases significantly compared with that at the age of 7 days. The maximum strength growth rate is 108.3%, and the average strength growth rate is 34%, indicating that the compressive strength of sludge baking-free brick is significantly affected by age. The growth of compressive strength mainly occurs after the age of 7 days. The incorporation of sludge particles affects the hydration rate of cement and delays the strength growth of the baking-free brick [22].



**Figure 5:** Effect of different sludge content and water-binder ratio on the compressive strength of baking-free bricks at 7 and 14 days

With the increase of sludge content, the compressive strength of each sample showed a decreasing trend. With the gradual increase of the water-binder ratio, the compressive strength of the experimental group with sludge content of 10% increased linearly. In the experimental group with a sludge content of 30%, the compressive strength increased first and then decreased. The increase of compressive strength was not apparent in the experimental group with a sludge content of 50%. It shows that when sludge particles are directly added as fine aggregate, the compressive strength of baking-free brick is obviously affected by the amount of mixing water, so a reasonable water-binder ratio should be adjusted or compensatory water should be added.

The 7d compressive strength of the DZ group is 31.26 MPa, which is much higher than that of the sludge baking-free brick samples at the same age. Among them, the strength loss rate of the sludge baking-free brick is 32.6%, the sludge particle content is 10%, the maximum strength loss rate is 91.8%, and the strength deterioration is apparent. It is also higher than the compressive strength at the age of 14 days. It is necessary to maintain the design strength of the brick by controlling the sludge content.

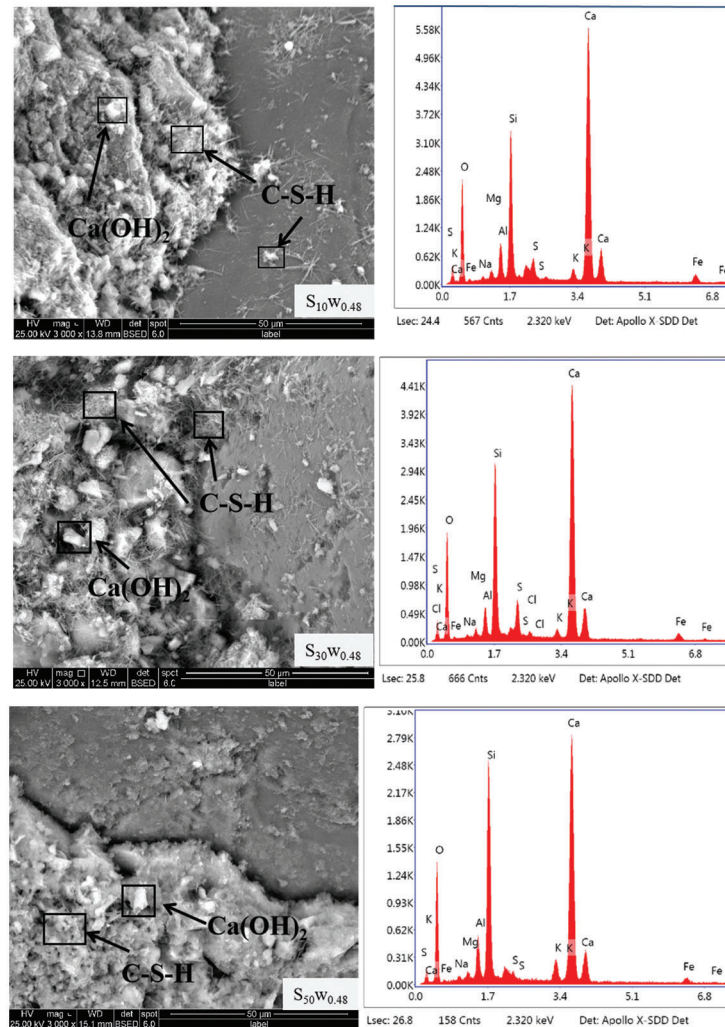
### 3.1.2 Microscopic Phase Analysis

Fig. 6 shows the microscopic morphology of samples with different sludge content. SEM images of sample series with the water-binder ratio of 0.48 and 3000 times were selected for analysis. It can be found that there are apparent differences in the mortar phase morphology of the  $S_{10}W_{0.48}$  group,  $S_{30}W_{0.48}$  group, and  $S_{50}W_{0.48}$  group, and the development degree of hydration products is different. The hydration products were analyzed by EDS. The main elements were Ca, Si and O, and the hydration products were speculated to be C-S-H gel and  $Ca(OH)_2$  crystal by diffraction peaks of elements. The  $S_{10}W_{0.48}$  group of C-S-H gel interlaced with each other, covered the surface of the matrix, filled the void between cement particles, and had a relatively compact structure. The amount of C-S-H gel in the  $S_{30}W_{0.48}$  group was less and accumulated on  $Ca(OH)_2$  crystal, with some pores in the middle and the overall compactness is poor. The hydration products in the  $S_{50}W_{0.48}$  group were less and there were pores among hydration products, with poor overall connectivity. At the same time, it can be seen from the energy spectrum that the peak value of the Ca-Si spectrum decreases gradually with the increase of sludge dosage, indicating that the generated C-S-H gradually decreases. The sludge content affects the degree of cement hydration, which leads to a decrease in the macroscopic mechanical properties of baking-free bricks.

Fig. 7 shows the microscopic morphology of baking-free brick samples with different water-binder ratios. Sample series with sludge content of 30% and electron microscope images of 3000 times were selected for analysis.

Compared with the microscopic morphology of  $S_{10}W_{0.48}$ ,  $S_{30}W_{0.48}$ , and  $S_{50}W_{0.48}$  samples, the number of C-S-H gel and  $Ca(OH)_2$  crystals decreased with the increase or decrease of the water-gel ratio, and the overall connectivity decreased. Compared with the  $S_{30}W_{0.48}$  group, the Ca-Si spectrum peaks of the  $S_{30}W_{0.42}$  and  $S_{30}W_{0.54}$  groups decreased, indicating that the water-binder ratio also affected the hydration reaction of cement. It can be found that the hydration products are affected by the sludge content and water-binder ratio, which is consistent with the change law of macroscopic compressive strength. It shows that there is an optimal ratio between sludge content and water-binder ratio.

In summary, it is further concluded that the compressive strength of the brick is mainly affected by the water-binder ratio when the sludge content is less than 30%. Furthermore, when the sludge content is more than 30%, it is mainly affected by the sludge content, followed by the water-binder ratio.



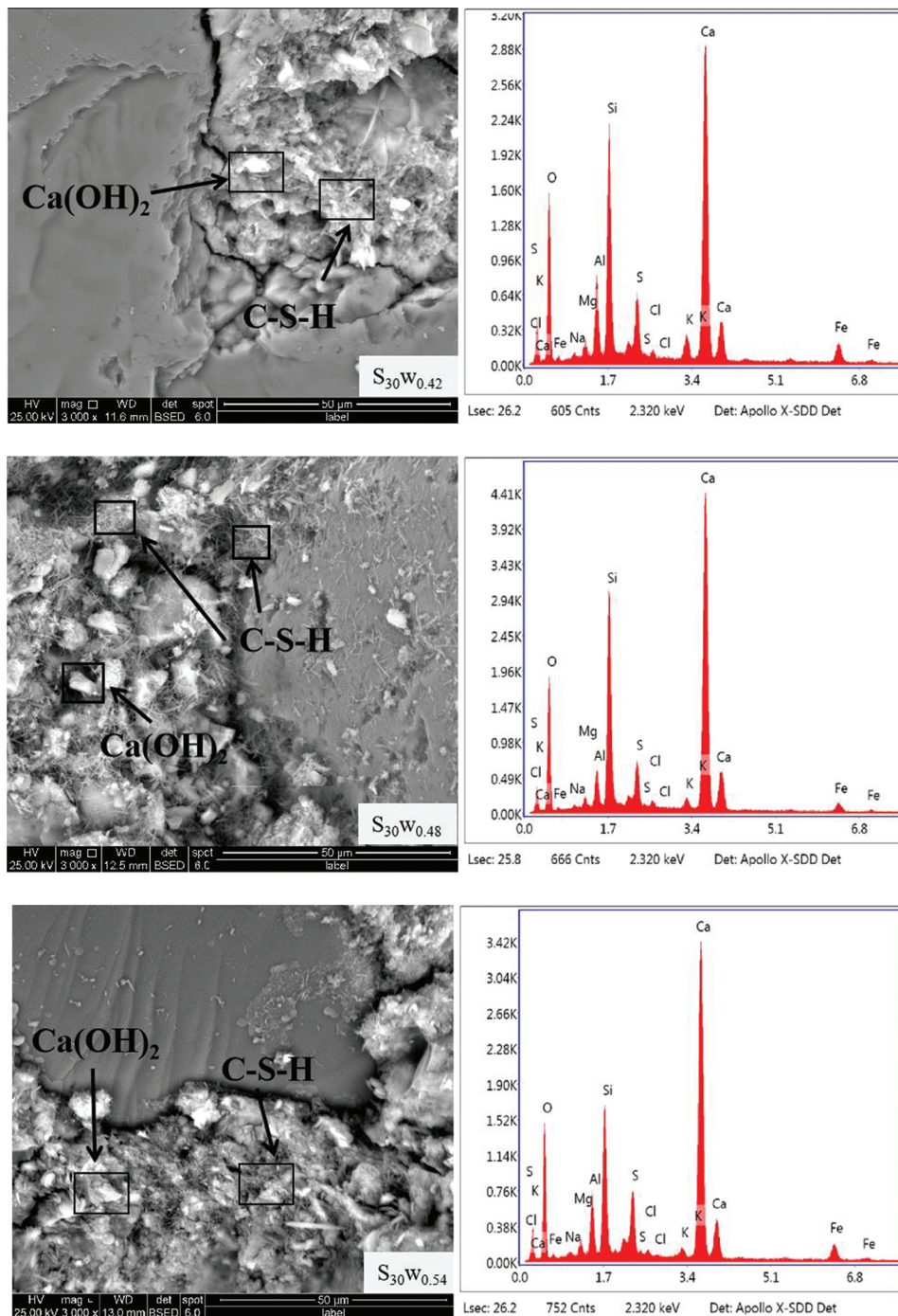
**Figure 6:** Microscopic morphology of baking-free brick samples with different sludge content (water-binder ratio 0.48,  $\times 3000$ )

### 3.2 Influence of Sludge WSAs Content on Properties of Baking-Free Brick

#### 3.2.1 Compressive Strength

According to the preliminary experimental study of our research group, the proportion of aggregate core components was sludge:cement:slag = 50%:25%:25%. The aggregate prepared with a molding time of 20 min and curing age of 28 days has the best performance. According to the requirements of artificial light aggregate in the specification “Light Aggregates and Test Methods” (GB/T L7431.1-2010) [23], the artificial aggregate prepared can be determined to be grade 700, as shown in Table 7.

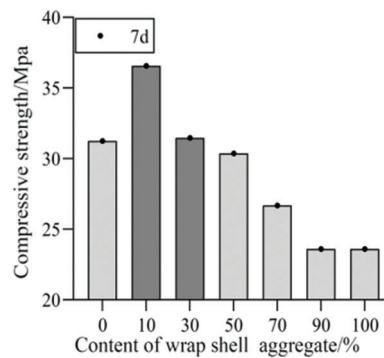
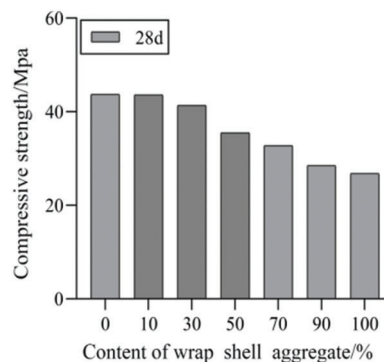
Figs. 8 and 9 show the influence of different sludge WSAs contents on the compressive strength of the bricks at 7 and 28 days.



**Figure 7:** Microscopic morphology of baking-free brick samples with different water-binder ratios (30% sludge content,  $\times 3000$ )

**Table 7:** Reference standard requirements

Artificial light aggregate	Density grade	Density range/ $\text{kg}\cdot\text{m}^{-3}$	Cylinder pressure strength/MPa	Water absorption of 1 h/%	Average grain shape coefficient
	600	>500, ≤600	2.0	≤10%	≤2.0
	700	>600, ≤700	3.0	≤10%	≤2.0

**Figure 8:** The influence of different WSAs contents on the compressive strength of baking-free brick at 7 days**Figure 9:** The influence of different WSAs contents on the compressive strength of baking-free brick at 28 days

For 7 days age, the compressive strength of experimental group S0 is 31.26 MPa, and the compressive strength of S10 and S30 groups are 36.57 and 31.48 MPa, respectively, which are higher than that of the S0 group. The compressive strength of experimental group S50 is 30.38 MPa, and the loss of compressive strength is lower than that of the S0 experimental group. At the age of 28 days, the compressive strength of experimental groups S10–S100 showed a step-down trend as the replacement rate of WSAs increased, and the strength of experimental groups S100 decreased by 24.5% compared with that of S0 experimental groups. It shows that in the ages of 7 days are added as wrap shell replace gravel aggregate, in the case of guarantee replacement rate is reasonable, not only can effectively guarantee the early strength of baking-free brick, but also improve baking-free brick early strength effect, which can shorten the maintenance cycle and improve the product turnover rate for baking-free brick products, and at the same time effectively guarantee the quality of products.

For 28 days age, the compressive strength of the S0 experimental group is 43.7 MPa, and the strength growth rate is close to 40%, while the strength growth rate of the S10–S100 experimental group is 15%–30%. The maximum strength of the S10 experimental group is 43.6 MPa, which is almost close to S0 experimental group and the strength of the S30 experimental group is 41.4 MPa. The strength loss rate is about 5%, which still maintains the ideal compressive strength. With the increase of WSAs replacement rate, the compressive strength trend of the baking-free brick is consistent with that of the 7 days age, showing a decreasing change law. The compressive strength of the S50 experimental group is 35.5 MPa, which can also meet the application requirements of baking-free bricks.

Fig. 10 shows the destructive patterns of baking-free brick in different experimental groups. It can be found that the damaged surface of all experimental groups showed a residual fracture of WSAs, which became more obvious with the increase in replacement rate, indicating that the strength of WSAs was significantly different from that of gravel after the addition of WSAs, resulting in a weak strength zone. In the case of compression, the damage first occurs around the weak area, and then cracks are formed along the damaged surface, leading to the damage to the baking-free brick.

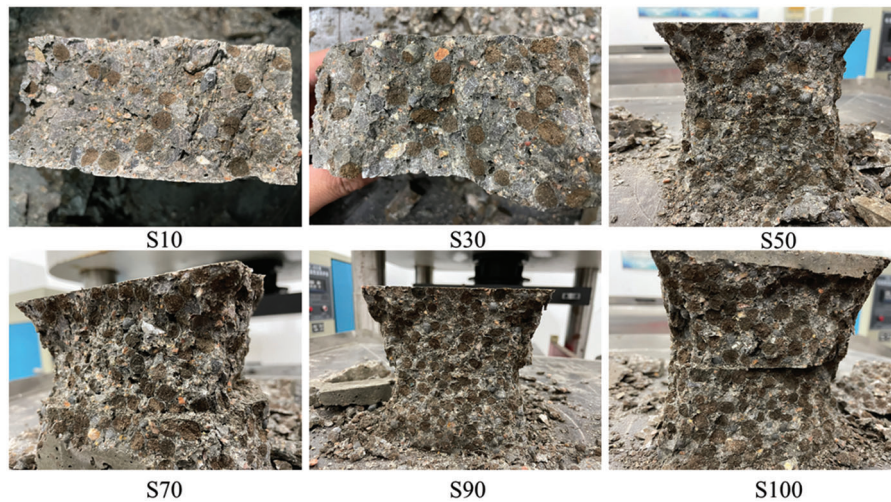


**Figure 10:** Failure mode of baking-free brick sample

### 3.2.2 Water Bibulous Rate

Fig. 11 shows the curve of the maximum water absorption rate of 28 days age baking-free brick. It can be seen from the figure that the water absorption rate of experimental groups S0~S100 showed a trend of step increase. The S10 group was the closest to the S0 group, with a water absorption rate of 5%–6%. The water absorption rate of the S30 and S50 experimental groups increased, by around 7%–8%. The water absorption rates of the S70~S100 experimental groups were all greater than 11%. According to the test results of the water absorption rate of WSAs, compared with natural gravel, the water absorption rate of WSAs itself is higher, and the 1 h water absorption rate is between 10% and 15%. Therefore, with the increase of replacement rate, the baking-free brick water bibulous rate is gradually increased, and the reason for the step-up may be due to the WSAs and gravel system making the internal dense degree of baking-free brick is different.

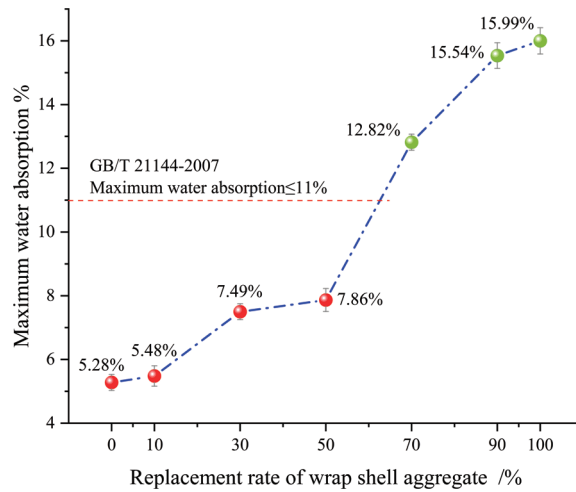


**Figure 11:** Maximum water absorption rate of baking-free bricks at 28 days age

### 3.2.3 Pore Structure

#### NMR Pore Structure Analysis

Figs. 12 and 13 show the NMR pore size distribution and pore throat distribution of the baking-free brick, respectively.

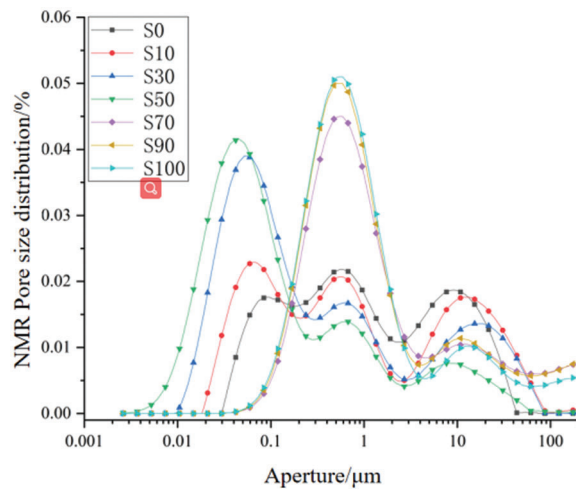


**Figure 12:** NMR pore size distribution of baking-free brick (0~200 μm)

From the pore size distribution diagram in Fig. 12, it can be seen that there are two stages of changes in the pore size distribution pattern from S10 to S100 relative to the S0 experimental group. In the first stage, from S10 to S50 experimental groups, the pore size distribution curve above 0.1 μm gradually decreased, and the pore size distribution curve below 0.1 μm gradually increased, indicating that when the content of WSAs was less than 50%, the holes above 0.1 μm in the brick were reduced and transformed into smaller holes. In the second stage, from S70 to S100 experimental groups, the pore size distribution curve changed from 3 main peaks to 2 main peaks, and the pore size distribution mainly ranged from 0.1 to 2.5 μm.

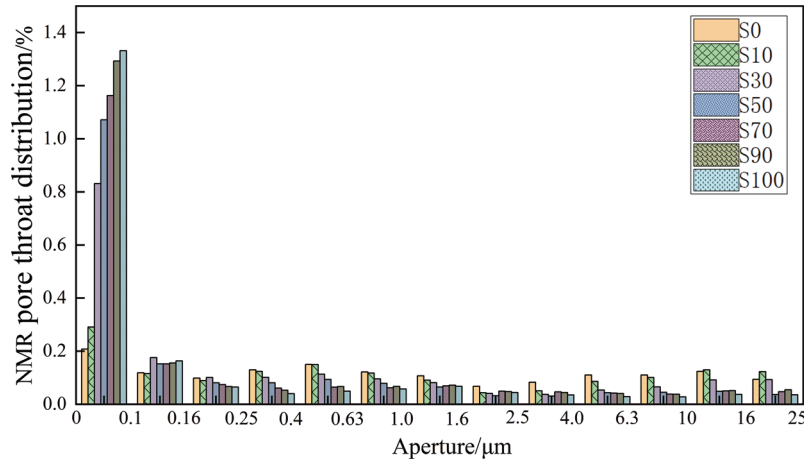


**Figure 13:** NMR pore throat distribution map of baking-free brick (0~25 μm)

Pore throat refers to the narrow interconnecting channels between pores in rock mass or soil. As can be seen from the NMR pore throat distribution diagram in Fig. 13, the variation of pore throat distribution in all experimental groups is mainly concentrated below 0.1 μm, which shows a significant increasing trend, while the pore throat distribution in other pore throat regions gradually decreases, and the overall change is not apparent. According to the model proposed by Bute [24], the pores are divided into gel pores (<10 nm), transition pores (10–100 nm), capillary pores (100–1000 nm), and macropores (>1000 nm). After the addition of WSAs, the capillary pores and macropores of baking-free bricks decrease, while transition pores and gel pores increase.

*PCAS Flat Face Results Analysis*

Fig. 14 shows the variation of porosity and fractal dimension of the flat face of the baking-free brick. From the results, the plane porosity of the bricks also shows a decreasing trend, and the decrease is more obvious than that of the S0 experimental group. At the same time, the fractal dimension is also relatively reduced, indicating that the hole shape of the flat face is also optimized, which is because of the spherical WSAs. When the gravel aggregate is replaced, there will be an optimal aggregate space. At the same time, the spherical aggregate has a morphological effect, which can improve the workability of the baking-free brick and make the baking-free brick denser.

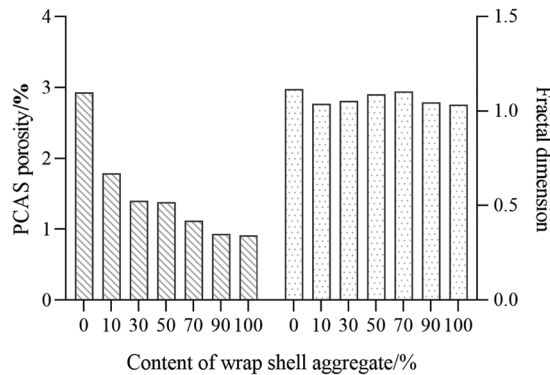


**Figure 14:** Plane porosity and fractal dimension of baking-free brick

In summary, the results show that the addition of WSAs is beneficial to improving the internal pore structure of the bricks and reducing the porosity of specimens. The porosity and pore structure distribution inside the specimen are important factors affecting the mechanical properties of cement-based materials. Therefore, the gradually optimized pore structure can enhance the mechanical properties of the specimen under the condition that the content of WSAs is designed reasonably.

Under the condition of a reasonable replacement rate, sludge WSAs can not only improve the early strength of brick, improve the turnover rate of brick building materials, but also improve the pore structure and optimize the pore characteristics of the brick body. It can be seen that sludge WSAs instead of natural aggregate can not only solve the problems of sludge deposition, reduce environmental pollution, alleviate the serious exploitation of natural aggregate resources, but also be used as building materials products in the field of building materials.

#### 4 Mechanism of the Effect of Sludge WSAs on Baking-Free Bricks

The method of extracting flat face structure with the help of PCAS software [25] is used to extract the section possession map of WSAs on the cutting surface of the baking-free brick, as shown in Fig. 15.

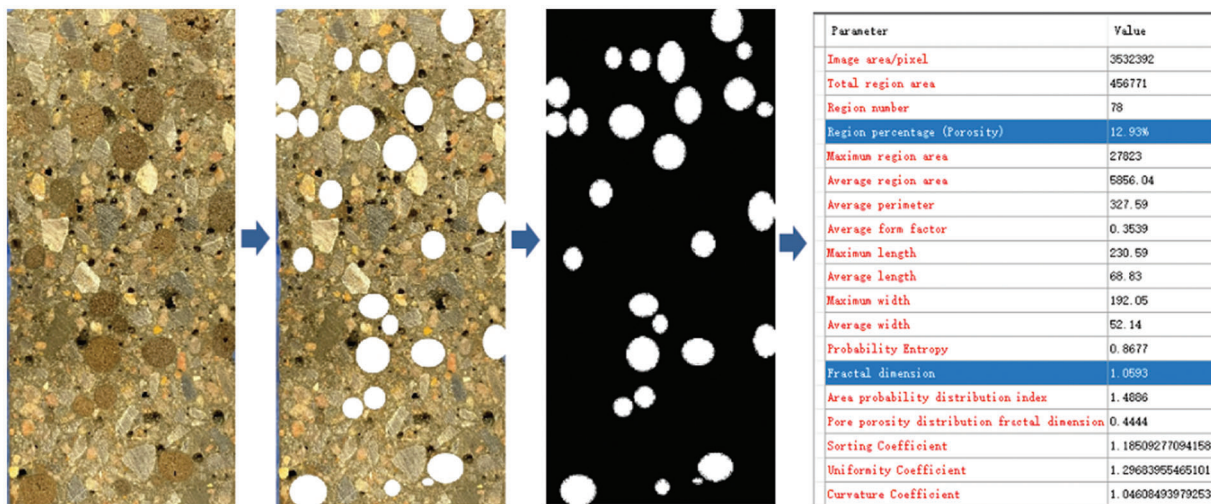


**Figure 15:** Calculation process of the occupancy rate of the WSAs section

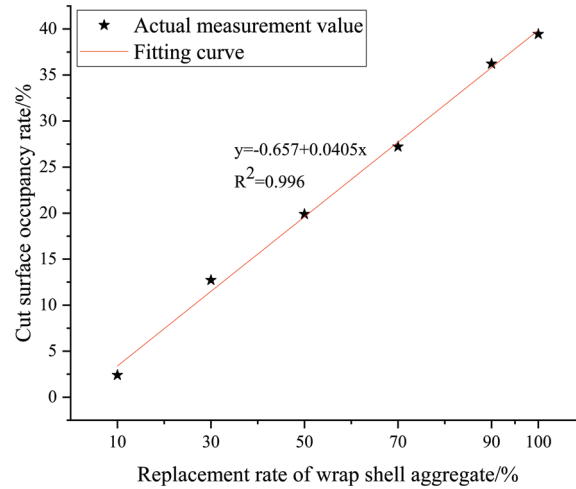
Fig. 16 shows the fitting curve of the relationship between WSAs replacement rate and occupancy rate of the cut surface. If the replacement rate of WSAs is used as the design index of the three-dimensional sample ratio, the cut surface occupancy rate of WSAs can be used as the design index of the two-dimensional section. The linear fitting results were good, and  $R^2$  was 0.996, indicating that the fitting results of trend lines were reliable. Conversion of three and two dimensional design indexes based on the linear model could provide a theoretical basis for numerical simulation research.

Fig. 17 shows the fitting results of cut section occupancy rate of WSAs and compressive strength of baking-free bricks. The results of linear fitting are ideal for both ages. The linear model is shown in the following equation:

$$y_7 = 36.87 - 0.355x$$

$$y_{28} = 45.65 - 0.473x$$

where,  $y$  is the compressive strength of the baking-free brick, MPa.  $x$  is the cut section occupancy rate of WSAs, %.



**Figure 16:** The relationship between the replacement rate of WSAs and the cut surface occupancy rate

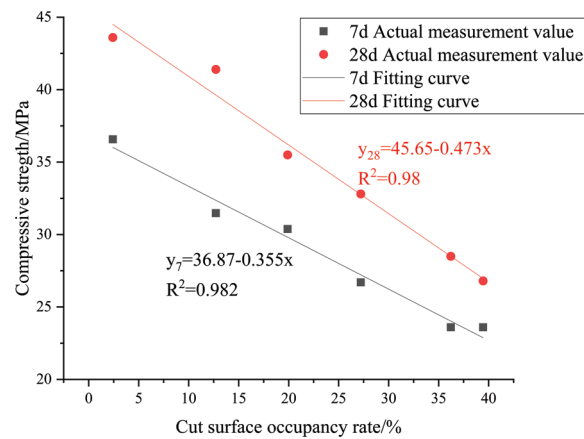
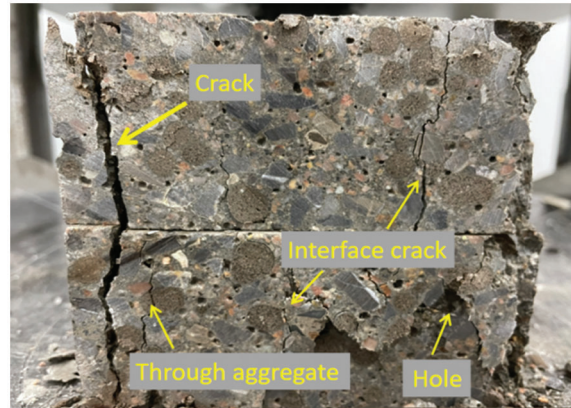


**Figure 17:** The relationship between the cut surface occupancy rate of the WSAs and the compressive strength of the baking-free brick

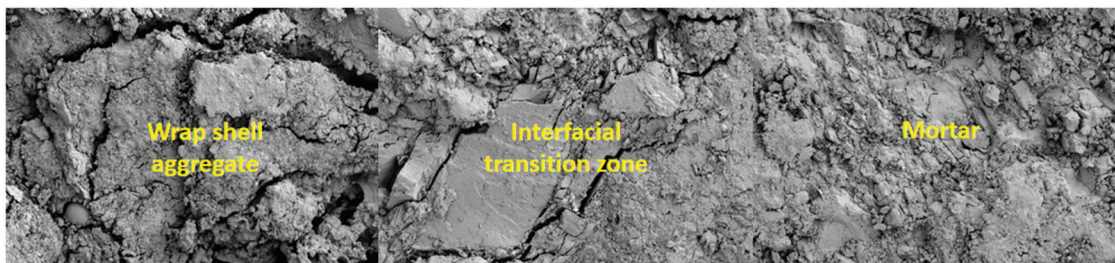
The content of WSAs is the main factor affecting the compressive strength of brick, while the strength prediction and test ratio design can be initially carried out according to the linear model. Fig. 18 shows the cut surface morphology of the baking-free brick. It can be observed in the figure that the location of damage occurring after the destruction of the baking-free brick specimen is mainly concentrated around the WSAs, with cracks through the WSAs and cracks around the WSAs interface, which can further illustrate the mechanism of the influence of the cut surface occupancy rate on the compressive strength of the baking-free brick, the larger the cut surface occupancy rate, the more possible damage locations appear and the cracks accumulate to eventually cause damage [26,27].

Fig. 19 shows the microscopic morphology of WSAs baking-free brick. It can be seen from the figure that WSAs-interface transition zone-mortar form obvious morphological characteristics. The internal microstructure of WSAs is loose, with the obvious distribution of cracks and pores and the degree of hydration is low. There are also multiple systems of “aggregate core-shell-mortar” in the interface transition zone. There are still gaps in the interface binding position, with the low binding degree and stratified state. The mortar matrix is dense and highly hydrated [28,29]. This is completely consistent

with the prediction conclusion of the sectional damage mode of the baking-free brick in Fig. 19. For WSAs baking-free brick, the damage is more likely to occur in WSAs and interface transition zone.



**Figure 18:** Destruction pattern of baking-free brick cut surface



**Figure 19:** Micro morphology of WSAs baking-free brick

In order to clarify the microstructure of WSAs baking-free brick, the microstructure of WSAs baking-free brick was compared with that of gravel aggregate baking-free brick. Fig. 20 shows the topography of gravel aggregate baking-free brick. As shown in Fig. 20, the gravel aggregate-interface transition zone-mortar three-phase system is also formed, with the difference of dense and complete gravel body. The interface transition zone between the gravel and the mortar phase is relatively close, which is not very different from the mortar body, so it has good strength. When gravel aggregate is replaced, the compressive capacity of baking-free brick is relatively weakened.

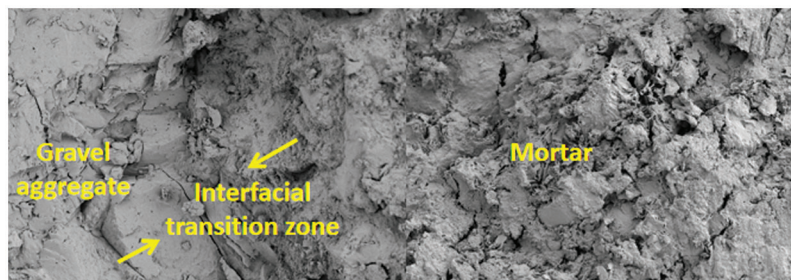


**Figure 20:** Morphology of crushed stone aggregate baking-free brick

To sum up, in order to make better application of WSAs, the internal compact-degree of WSAs should be improved. In addition, the combination degree between the aggregate core-shell, and shell-mortar should

be improved, and the elimination of the strength difference between WSAs and gravel aggregate is more conducive to the wide use of WSAs.

## 5 Conclusion

In this study, leather industrial sludge was used as raw material to prepare WSAs with ideal properties. The application of sludge and its WSAs instead of sand in baking-free brick was studied. Additionally, the influence of the different amounts of aggregate replacement on the properties of baking-free brick was investigated. According to the research data, the following conclusions are drawn:

- (1) There is an optimal replacement amount of sludge and WSAs. When the sludge content is less than 30%, it is mainly affected by the water-binder ratio. When the sludge content is more than 30%, it is mainly affected by the sludge content.
- (2) When the replacement amount of WSAs is less than 30%, the early strength of the baking-free brick can be improved, the curing cycle can be shortened, and the product turnover can be improved. A reasonable aggregate replacement rate can refine the porosity and reduce the plane porosity of the bricks.
- (3) The three-phase system of WSAs-interface transition zone-mortar is poorly bonded compared with the gravel aggregate-interface transition zone-mortar system. The WSAs and interface transition zone-mortar system are more prone to damage.
- (4) For the better application of WSAs, the internal compactness of WSAs should be improved on the one hand, and the bonding degree between the core-shell and shell-mortar should be improved on the other hand. It has broad application prospects and market value to prepare baking-free brick with reasonable replacement of sludge and WSAs.

**Data Availability Statement:** All data, models, and code generated or used during the study appear in the submitted article.

**Funding Statement:** This study was funded by the Natural Science Foundation of Henan Province (202300410270); Graduate Education Innovation Program fund of North China University of Water Resources and Electric Power (YK-2021-49).

**Conflicts of Interest:** The authors declare that they have no conflicts of interest to report regarding the present study.

## References

1. Han, J. X., Xiao, X. Y. (2013). Current situation and development trend of aggregate in China. *Concrete World*, 51(9), 36–42.
2. Yuan, X. S., Gao, H., He, Z. S., Zhang, Z. S., Yan, M. J. (2020). Metrological analysis and future prospect of documents related to sludge treatment and disposal technology in China. *Pearl River*, 41(10), 102–108.
3. Wang, P., Tang, C. S., Sun, K. Q., Chen, Z. H., Xu, S. K. et al. (2016). Research progress of solidification/stabilization technology for sludge treatment. *Journal of Engineering Geology*, 24(4), 649–660.
4. Kaosol, T. (2010). Reuse water treatment sludge for hollow concrete block manufacture. *Energy Research Journal*, 1(2), 131–134.
5. Liu, Y., Zhuge, Y., Chow, C. W., Keegan, A., Li, D. et al. (2020). Utilization of drinking water treatment sludge in concrete paving blocks: Microstructural analysis, durability and leaching properties. *Journal of Environmental Management*, 262, 611–620.
6. Baeza-Brotons, F., Garcés, P., Payá, J., Saval, J. M. (2014). Portland cement systems with addition of sewage sludge ash. Application in concretes for the manufacture of blocks. *Journal of Cleaner Production*, 82(7), 112–124. DOI 10.1016/j.jclepro.2014.06.072.
7. Hameed, M. S., Sekar, A. S. S., Balamurugan, L., Saraswathy, V. (2012). Self-compacting concrete using marble sludge powder and crushed rock dust. *KSCE Journal of Civil Engineering*, 16(6), 980–988. DOI 10.1007/s12205-012-1171-y.

8. Ni, Y. L., Lan, M. Z., Cui, J. X., Di, Y., He, J. (2022). Experimental study on preparation of sintered brick from river and lake silt. *New Building Materials*, 49(1), 94–97+107.
9. Le, H. A., Oanh, N. T. K. (2020). Integrated assessment of brick kiln emission impacts on air quality. *Environmental Monitoring and Assessment*, 171(1–4), 381–394.
10. Uma, R., Vasudev, A., Santhosh, R., Sameer, M., Dheeraj, L. (2014). Assessment of air pollutant emissions from brick kilns. *Atmospheric Environment*, 98(10), 549–553.
11. Guo, L., Chen, P. P., Guo, L. X., Xue, Z. L., Guan, Z. et al. (2021). Pore structure characteristics of baking-free slag-sludge bricks and its correlations to mechanical properties. *Journal of Renewable Materials*, 9(10), 1805–1819. DOI 10.32604/jrm.2021.015140.
12. Miqueleiz, L., Ramirez, F., Oti, J. E., Seco, A., Kinuthia, J. M. et al. (2013). Alumina filler waste as clay replacement material for baking-free brick production. *Engineering Geology*, 163(8), 68–74. DOI 10.1016/j.enggeo.2013.05.006.
13. Liu, J. C., Zhu, L. (2018). Study on durability of silt-baking-free brick. *Bulletin of the Chinese Ceramic Society*, 37(12), 3816–3820.
14. Lu, M., Xiong, Z. H., Lin, X., Fang, K. J., Li, J. Q. et al. (2019). Effect of additives on properties of waste incineration slag baking-free brick. *Environmental Chemistry*, 38(9), 2141–2148.
15. Ji, W. J., Liu, Y., Li, Z. (2019). Study on the preparation process of baking-free bricks with red mud and fly ash. *Journal of North University of China (Natural Science Edition)*, 40(6), 568–572.
16. GB/T 21144-2007 (2008). Concrete solid brick.
17. GB/T 4111-2013 (2014). Test method for concrete blocks and bricks.
18. Liu, C., Shi, B., Zhou, J. (2011). Quantification and characterization of microporosity by image processing, geometric measurement and statistical methods: Application on SEM images of clay materials. *Applied Clay Science*, 54(1), 97–106. DOI 10.1016/j.clay.2011.07.022.
19. Yan, G. Y., Wei, Z. T., Song, Y., Zhang, J. J., Yang, H. (2018). Quantitative characterization of shale pore structure based on AR-SEM and PCAS. *Earth Science*, 43(5), 1602–1610.
20. Miao, C. Y., Yang, L., Xu, Y. Z., Yang, K., Zhao, W. C. et al. (2014). Experimental study on strength softening behaviors and micro-mechanisms of sandstone based on nuclear magnetic resonance. *Chinese Journal of Rock Mechanics and Engineering*, 40(11), 2189–2198.
21. Wang, K., Zhou, H. Y., Lai, J., Wang, K. J., Liu, Y. (2020). Application of NMR technology in characterization of petrophysics and pore structure. *Chinese Journal of Scientific Instrument*, 41(2), 101–114.
22. Hong, M. N., Li, N., Feng, X. J., Zhan, J. R., Wu, Y. (2020). The influence of different dosage of composite cementitious materials on the properties of unburned wrapped shell aggregate in dredged sediment. *New Building Materials*, 47(7), 4–8.
23. GB/T 17431.1-2010 (2010). Lightweight aggregates and Its test methods-Part 2: Test methods for lightweight aggregates.
24. Guo, J. F. (2004). *Theoretical study on the relationship between concrete hole structure and strength*. Zhejiang University.
25. Huang, W. B., Li, X., Song, J., Zhao, Z., Li, Z. J. (2019). Microcosmic determination method of coastal soft soil. *Science Technology and Engineering*, 19(28), 290–296.
26. Tian, T., Zhang, L. Y., Li, Y. S. (2019). Performance analysis of non-sintered aggregate bricks prepared with dredged sediment through wet process. *Journal of Tianjin University of Science and Technology*, 34(5), 63–67,80.
27. Yang, P. G., An, X. R., Peng, Y. Z. (2018). Study on performance of concrete pavement brick with dredged sediment non-sintered wrap shell aggregates. *New Building Materials*, 45(7), 6.
28. Huang, Y., Hu, X., Shi, C. J., Wu, Z. M. (2022). Review on formation and improvement of interface transition zone between cement slurry and aggregate in concrete. *Journal of Materials Review*, 37(1), 1–22.
29. Xiang, Z. C., Li, Y., Shen, Z. H. (2021). Mechanical properties of mortar aggregate interface. *Journal of Hubei University of Technology*, 36(5), 91–95+116.